

EXPERIMENTAL STUDY OF WING STRUCTURE GEOMETRY TO MITIGATE PROCESS-INDUCED DEFORMATION

Justin D. Valenti^{*‡}, Joseph Bartolai[†], and Michael A. Yukish^{*}

^{*}Department of Aerospace Engineering

[†]Applied Research Laboratory

The Pennsylvania State University, University Park, PA

Abstract

Small uncrewed aerial vehicles that are fabricated with material extrusion additive manufacturing often have wings that are single-perimeter structures with sparse internal structure. The large distance between internal supports creates an “unsupported-wall distance”, which leaves the wing skin prone to deformation during fabrication. This work explores and quantifies the relationship between the deformation of the wing skin and three geometric parameters: (1) unsupported-wall distance, (2) local surface curvature, and (3) extrusion width. A three-level full factorial study was devised in which wing sections of varying surface curvature, unsupported-wall distance, and extrusion width were fabricated with polymer material extrusion additive manufacturing. The surfaces of the wing sections were then digitized into point clouds with a coordinate measuring machine, and the point cloud data were directly compared to the GCode used to print each wing section. The deformation data was analyzed to quantify the relationship between deformation and the experimental parameters. From the experiment, a non-dimensional term was identified that captures a bounding relationship between the geometric parameters and the deformation. Finally, a mathematical expression was developed to serve an upper bound on unsupported-wall distance based on extrusion width and surface curvature.

Introduction

Additive manufacturing (AM) has emerged as a valuable new fabrication method for small uncrewed aerial vehicles (UAVs). The design freedom provided by AM has both simplified UAV fabrication and made new families of structure practical to fabricate. While several polymer AM processes have been used to build UAVs or UAV parts [1–11], the low-price point and ubiquity of polymer material extrusion additive manufacturing (MEAM) has led to many UAVs that were designed and built with MEAM [4, 12–27].

The high strength-to-weight requirement of wing structures, combined with the minimum feature size of most desktop 3D printers, typically leads to MEAM wings that have a single perimeter, with sparse internal structure. Additive manufacturing is known to struggle with this type of structure.

Previous work by the authors developed a structural design method that produced wing structures for small MEAM-built wings [28]. While wings designed with this method were successfully flown, the main drawback was that the single-extrusion perimeters on the resulting wings would deform during fabrication due to lack of support. A study was conducted to

[‡]Corresponding Author: jdv5076@psu.edu

explore the tradespace of weight, aerodynamic performance, and structural performance [29]. The main conclusions of this study were:

- Undeformed wing skin provides significantly more bending inertia than required (for a standard desktop 3D printer with a 0.4mm nozzle diameter and the chosen sUAV: span = 4ft, weight = 1 lb).
- Spar spacing and skin curvature strongly affect skin deformation.
- Additional internal structure reduced deformation to a point where aerodynamic performance was minimally affected, with negligibly more additional weight than the baseline internal structure designed to only carry the flight loads.

The present work is a continuation of that initial study and aims to further characterize the relationship of geometric design parameters to wing skin deformation.

Novel Contribution: The results of the experimental study show a clear bounding relationship between deformation of the single extrusion perimeter and (1) unsupported-wall distance, (2) surface curvature, and (3) extrusion width. A non-dimensional “unsupported-wall index” is identified which captures a bounding relationship between the geometric parameters and deformation. Lastly, a mathematical expression is presented to serve as a design guideline for unsupported-wall distance based on curvature and extrusion width.

Layout of Paper: The following section provides the methods used to design the wing sections, design the experiment, and obtain and process the deformation data. This is followed by the Results section, which shows the absolute deformation results, non-dimensionalized deformation results which match a previous study, and the presentation of a single non-dimensional value which appears to characterize the problem. Then, a design constraint for thin-walled structures presented based on the study data and analysis. Finally a conclusion section offers a small discussion of the results, concluding remarks, and future work. A nomenclature section is also provided at the end of the manuscript.

Methods

Wing Design and GCode Generation: Custom software, named GWing, was developed to simultaneously design UAV wings and generate the GCode to build them. GWing was used to design the wing sections and generate the GCode used for this study. The software breaks wings into printable wing sections. Each wing section is fabricated with spanwise direction of the wing aligned with the build direction and the chordwise direction aligned with the X-axis of the build plate, as shown in Figure 1. A brim is used to promote adhesion to the build plate. A solid first layer is also used which both improves build plate adhesion and becomes a rib in the final wing structure. All subsequent layers consist of a single perimeter and the internal structure. In each layer, the single perimeter is printed first which corresponds to the desired airfoil. The internal structure is printed second and consists of one or more vertical members, which become spars in the final wing structure. The tool path for an arbitrary layer is shown in Figure 2(a).

Experimental Design: A three-level full factorial study was devised to test the effects of surface curvature, κ , spar spacing, d_x , and extrusion width, w_e , on the deformation of the perimeters during the fabrication process. A parameterized wing section is shown in

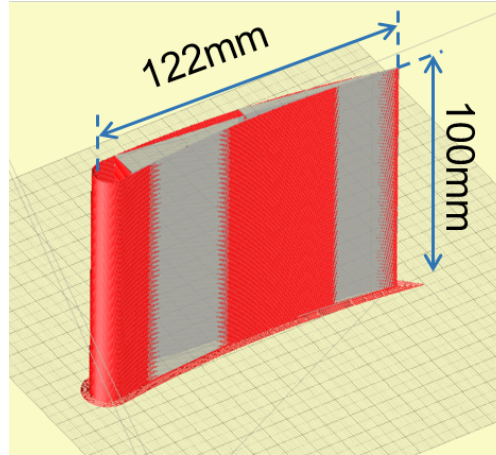


Figure 1: Example GCode of wing section, annotated with chord and section span dimensions. Extrusion moves are in red. Travel moves are shown in grey.

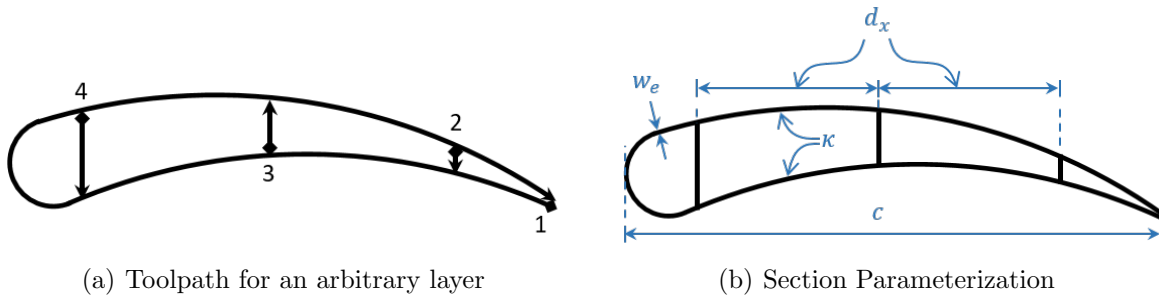


Figure 2: (a) Illustrates the toolpath for a layer of a wing section. The outer perimeter is extruded first, followed by the internal structure from the trailing edge to the leading edge. (b) Diagrams the parameterization of a wing section. Chord, c , was set to 122 mm for all wing sections in this study. Spar spacing, d_x , curvature, κ , and extrusion width, w_e , were the varied parameters in this study.

Figure 2(b). The wing shape and structure was constant for every layer. The chord for every section was 122mm.

Both the location and number of spars were defined by a single parameter, d_x , the spanwise distance between spars. The high aspect ratio of an airfoil section means that spar spacing is roughly equal to unsupported-wall distance, $d_x \approx d_u$. It is assumed that any effect on deformation from d_u will also appear with d_x . The three levels of spar spacing were $d_x = \{20, 50, 80\}$ mm.

Curvature is defined as the inverse of radius of curvature, $\kappa = 1/\rho$. For a given function $z(x)$, curvature is calculated

$$\kappa(x) = \frac{|z''|}{(1 + z'^2)^{(3/2)}}. \quad (1)$$

Note, the dimension of curvature is length^{-1} . While the curvature of a typical airfoil varies across the chord for both the upper and lower surfaces, airfoil sections for this experiment consist of circular arcs on both the upper and lower surface, as shown in Figure 2. The curvatures of both the upper and lower surfaces were equal. The three values of curvature

used were $\kappa = \{0, 2.5, 5\}\text{m}^{-1}$.

To maintain the proportions of nozzle diameter, extrusion width, and layer height across all test sections, three MEAM machines were used, each with a different nozzle diameter. A Lulzbot Mini 2 with a nozzle diameter of 0.25mm was used to fabricate sections with a design extrusion width $w_{e,d} = 0.31\text{mm}$ and a layer height $h_l = 0.17\text{mm}$. A Creality CR-10 with a nozzle diameter of 0.40mm was used to fabricate sections with a design extrusion width $w_{e,d} = 0.50\text{mm}$ and a layer height $h_l = 0.27\text{mm}$. A second Lulzbot Mini 2 with a nozzle diameter of 0.50mm was used to fabricate sections with a design extrusion width $w_{e,d} = 0.62\text{mm}$ and a layer height $h_l = 0.33\text{mm}$.

In summary, three parameters were varied at three levels to provide 27 test points, with the parameter levels being

$$\begin{aligned} d_x &= \{ 20, 50, 80 \}\text{mm}, \\ \kappa &= \{ 0, 2.5, 5 \}\text{m}^{-1}, \\ w_{e,d} &= \{ 0.31, 0.50, 0.62 \}\text{mm}. \end{aligned}$$

Sectional views of the variation in curvature and spar spacing are shown in Figure 3. A wing section was designed and fabricated for each point. The deformation of both the upper and lower surfaces were independently quantified, doubling the number of data points. The build parameters were:

- MEAM Machine*: { Lulzbot Mini 2, Creality CR-10, Lulzbot Mini 2[†] }
- Slicing Software: G Wing (custom, described above)
- Material: Polylactic Acid (Essentium PLA XTR Natural)
- Nozzle Diameter*: { 0.25, 0.40, 0.50 }mm
- Layer Height*: { 0.17, 0.27, 0.33 }mm
- Nozzle Temp: 210 deg C
- Bed Temp: 60 deg C
- Toolhead Speed: 40 mm/s

For the purposes of this study, differences between the three MEAM machines are assumed to be negligible.

Measurement: Calipers were used to measure the wall thickness of each section for both the upper and lower surfaces. This provided a “measured extrusion width”, $w_{e,m}$, to compare to the designed extrusion width, $w_{e,d}$. A laser coordinate measuring machine (CMM), specifically a FARO arm [30], was used to digitize the surface of each wing section in a point cloud. A wing section on the CMM table, along with the point cloud capturing its surface are shown in Figure 4.

Each point cloud was directly compared to the corresponding GCode file. For each point in a point cloud, a local deformation, δ , was calculated. The root mean square (RMS) of all deformation values for a particular section was calculated to provide an RMS deformation of the as-built part. This process is provided in Algorithm 1.

*Parameters listed in sets of three correspond, respectively, with the three $w_{e,d}$ values.

[†]Two separate Lulzbot Mini 2s were used. One with a nozzle diameter of 0.25 mm and the other with a nozzle diameter of 0.5 mm.

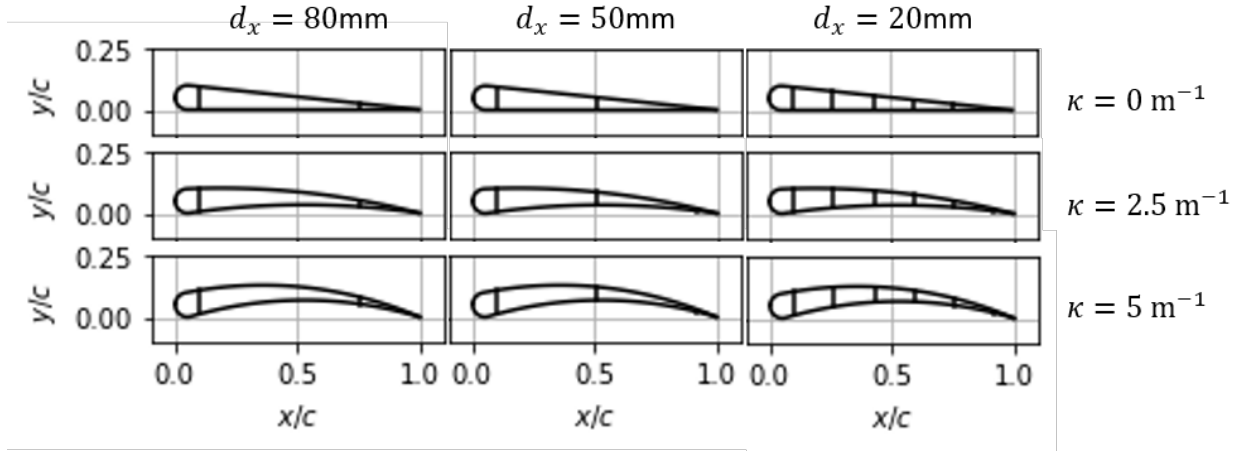


Figure 3: Three-level factorial design for unsupported-wall distance, d_x , and curvature, κ . The 9 design points illustrated above were each repeated 3 times for extrusion widths $w_{e,d} = [0.31, 0.50, 0.62]$ mm. For all wing sections, the chord $c = 122$ mm.

Algorithm 1: Compare a point cloud, defined by a list of points $P = (p_1, p_2, \dots, p_m)$, to a GCode file to calculate deformation of external surface of as-built part.

Input: GCode, Point Cloud

Output: RMS Deformation of As-Built Part

- 1 Convert Extrusion moves in GCode to list of points $G = (g_1, g_2, \dots, g_n)$;
 - 2 Align GCode points and point cloud;
 - 3 **for** each GCode Layer **do**
 - 4 Find all Point Cloud point within half a layers height;
 - 5 **for** Each Point Cloud Point, p_i , at the current layer **do**
 - 6 Find the closest GCode point at that layer, g_j to p_i ;
 - 7 Determine whether g_{j+1} or g_{j-1} is the next closest to p_i ;
 - 8 Calculate the local deformation, δ_i , defined as the perpendicular distance between p_i and the line defined by the two closest GCode points;
 - 9 **end**
 - 10 **end**
 - 11 Calculate the RMS of all δ values to find to RMS deformation of the as-built part ;
-

The RMS deformation provided the measure of a accuracy for a particular wing section and was used to quantify the deformation that occurred during the build process. The relationship between deformation and the design parameters is explored in the next section.

Results

Dimensional Results: First, the RMS deformation data, in millimeters, is plotted against the dimensional design parameters in Figure 5. To allow for the use of symbols to convey data, design extrusion width is used in Figures 5(a) and 5(b). Measured extrusion width is used in Figure 5(c). Clear bounding behaviors are shown in all three plots in Figure 5. Qual-

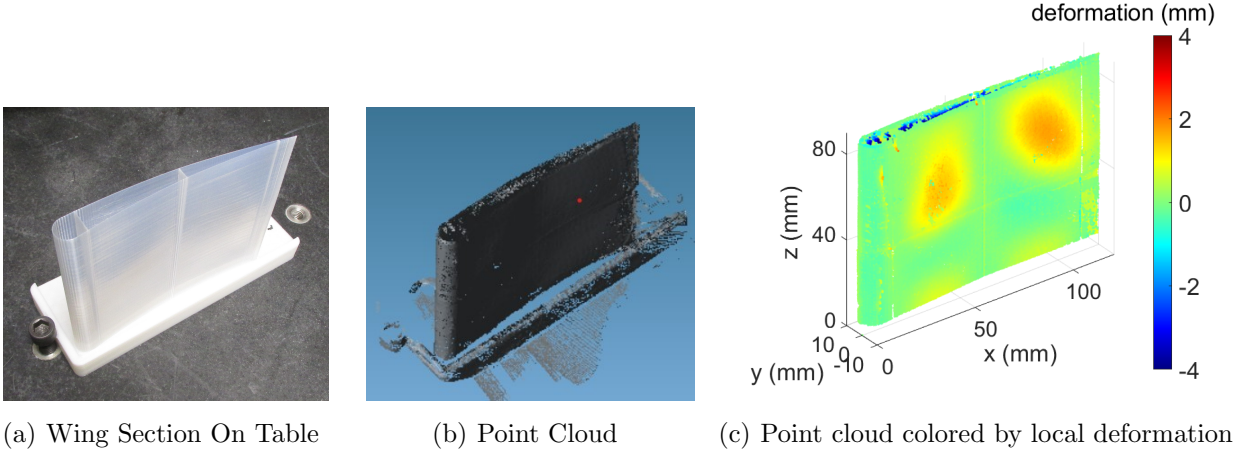


Figure 4: Example wing section from GCode illustrated in Figure 1. (a) The fabricated wing section on mounted on the CMM table awaiting measurement. (b) The point cloud generated by the CMM. (c) The point cloud with the deformation of each point from the intended GCode calculated.

itatively, it can be observed that as expected, RMS deformation increases with increased unsupported-wall distance, decreases with increased curvature, and decreases with increased extrusion width. Analysis of Variance (ANOVA) was performed to determine if the effects of spar spacing, curvature, and extrusion width on RMS deformation were statistically significant. The p-values of the three experimental parameters, as well as the interaction terms, are provided in Table 1. The small p-values indicate that the null hypothesis can be rejected. This suggests that all parameters and their interactions have a statistically significant affect on deformation.

Table 1: P-values of the three experimental parameters and their interaction terms.

Parameter	d_x	κ	$w_{e,d}$	$d_x \times \kappa$	$\kappa \times w_{e,d}$	$w_{e,d} \times d_x$
P-value	8.28e-13	6.04e-12	1.79e-9	2.87e-6	4.89e-6	7.80e-6

Non-Dimensional Results: In an effort to combine design parameters and simplify the problem, RMS deformation, unsupported-wall distance, and curvature were all non-dimensionalized by measured extrusion width. Both RMS deformation and unsupported-wall distance were divided by extrusion width. Curvature was multiplied by extrusion width, since the dimension of curvature is length^{-1} . Similar to the dimensional results, non-dimensional RMS deformation generally increases with non-dimensional unsupported-wall distance and generally decreases with non-dimensional curvature, as shown in Figure 6.

In an effort to further collapse the problem to a single dimensionless parameter, the unsupported-wall index, η , was conceived and is defined as

$$\eta = \left(\frac{\kappa}{d_x} \right) w_e^2. \quad (2)$$

Non-dimensional RMS deformation is plotted versus η in Figure 7. As with the rest of this work, plotting deformation versus unsupported-wall index does not show a clean curve, but

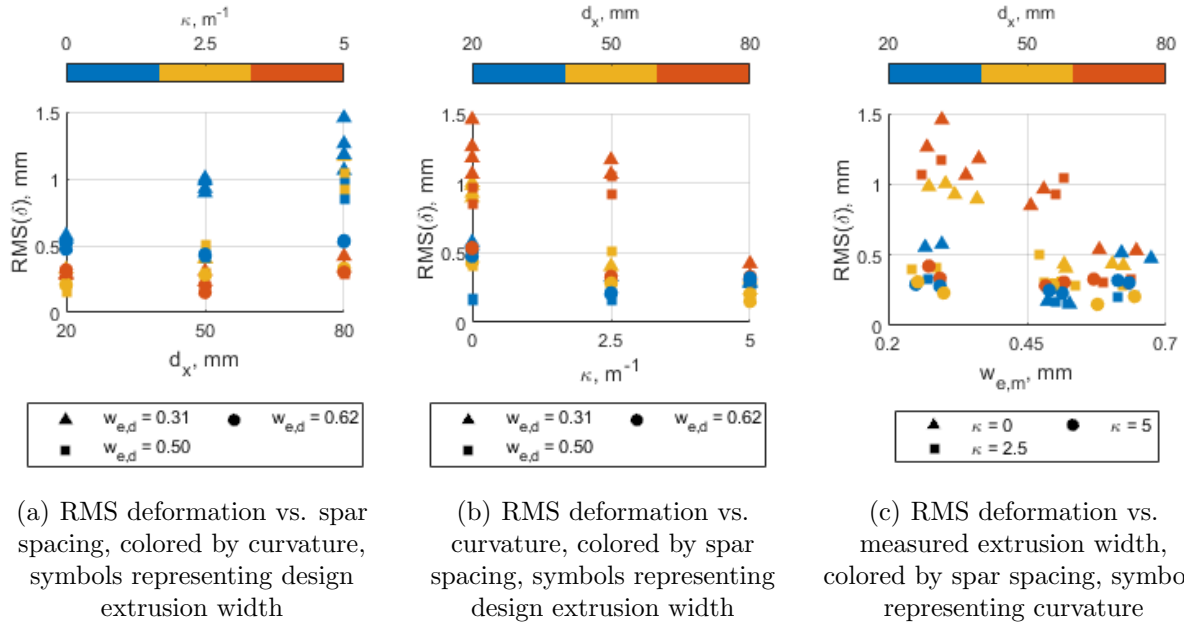


Figure 5: RMS deformation plotted versus the three design parameters. These plots show that, in general, deformation increases with spar spacing, decreases with curvature, and decreases with extrusion width.

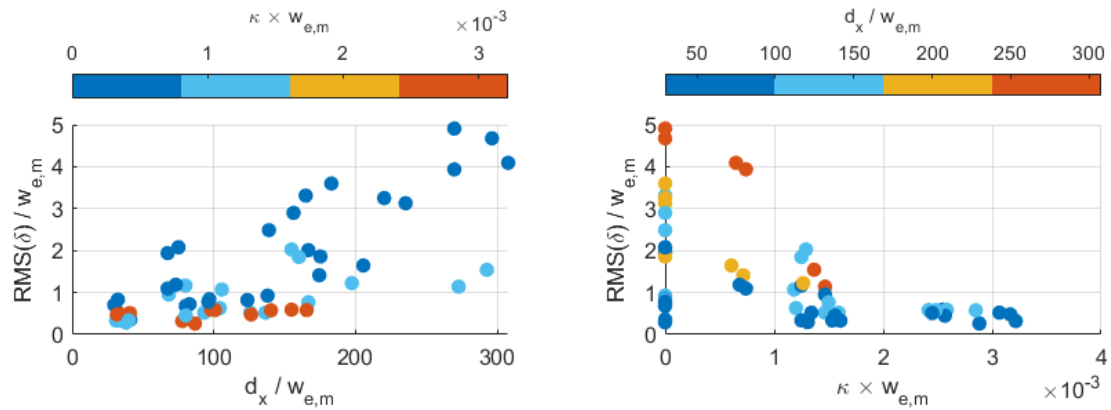


Figure 6: Deformation, spar spacing, and curvature non-dimensionalized by measured extrusion width. This allows the 3 dimensional design parameter to be collapsed to two non-dimensional parameters. The trends of the non-dimensional parameters match those of their dimensional counterparts.

more a bounding behavior. The deformation is bounded to relatively small amount above η values of roughly 2×10^{-5} and deformation has the potential to sharply increase below this η value.

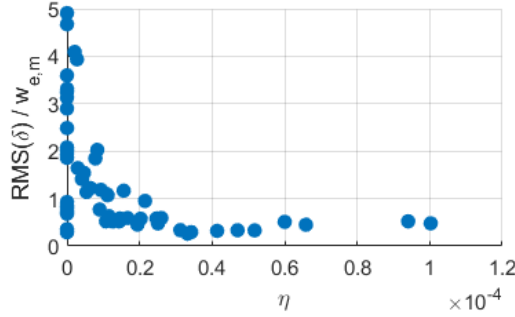


Figure 7: Non-dimensional deformation vs unsupported-wall index, defined by Equation 2. Index values above 2×10^{-5} yield relatively small deformations.

Proposed Design Guideline

A major goal of this research effort, beyond simply quantifying surface deformation, is to develop guidelines for designing MEAM-produced wing structures. When considering the three design parameters, d_u , κ , and w_e , the most easily varied parameter is d_u ; surface curvature is chosen based on desired aerodynamic performance and extrusion width is tied to nozzle diameter. Rearranging Equation 2 yields

$$d_u < \frac{1}{\eta^*} \kappa w_e^2 \quad (3)$$

where η^* is a critical unsupported-wall index. As noted in the previous section, the present study suggests 2×10^{-5} as reasonable value. Unfortunately, equation 3 drives unsupported-wall distance to zero as curvature goes to zero. Plotting non-dimensional deformation versus non-dimensional spar spacing, as shown in Figure 6(a), suggests that constraining the ratio of spar spacing to extrusion width to less than 50 yields an RMS deformation of less than one extrusion width. Translating this into a constraint on unsupported-wall distance yields

$$d_u < r^* w_e, \quad (4)$$

where r^* is a critical ratio of unsupported-wall distance to extrusion width. Combining the two constraints yields

$$d_u < \max \left[\frac{1}{\eta^*} \kappa w_e^2, r^* w_e \right]. \quad (5)$$

Equation 5 provides a constraint on unsupported-wall distance based on curvature and extrusion width. η^* and r^* are tuning parameters. Suggested values based on the present data are $[\eta^*, r^*] = [2 \times 10^{-5}, 50]$.

Conclusion

An experimental study was conducted to determine the effect of unsupported-wall distance, curvature, and extrusion width on the deformation of the skin of MEAM-produced wing sections during the fabrication process. While a precise mathematical function of the

design parameters for deformation could not be identified, the deformation data exhibited clear bounding behavior. The data showed that, in general, deformation increased with unsupported-wall distance, decreased with curvature, and decreased with extrusion width. Similar trends were identified when non-dimensionalizing deformation, unsupported-wall distance, and curvature by extrusion width. The results of an ANOVA study suggested that these trends were statistically significant.

Further non-dimensional analysis identified a dimensionless “unsupported-wall index”, η , which appears to collapse the problem to a single parameter. The wall deformation appears to be relatively small at higher η values.

Finally, a novel constraint on unsupported-wall distance was developed and presented in Equation 5. The expression constrains unsupported-wall distance based on curvature and extrusion width.

Future work will apply the new design constraint to different problems and explore the validity of the new design constraint. Additionally, there is work to be done to explore the physical mechanisms of deformation that were observed in the this study.

Acknowledgements

The authors would like to offer special thanks to Dr. Charlie Tricou, for his expertise in design of experiments and helping to conceive the origins of this work, and Dr. Callie Zawaski and Dr. Simon Miller for their many hours of discussion on this work and how to improve it.

References

- [1] S. K. Moon, Y. E. Tan, J. Hwang, and Y. J. Yoon, “Application of 3D printing technology for designing light-weight unmanned aerial vehicle wing structures,” *International Journal of Precision Engineering and Manufacturing - Green Technology*, 2014.
- [2] S. J. Furst, G. Bunget, and S. Seelecke, “Design and fabrication of a bat-inspired flapping-flight platform using shape memory alloy muscles and joints,” *Smart Materials and Structures*, vol. 22, no. 1, 1 2013.
- [3] C. Richter and H. Lipson, “Untethered hovering flapping flight of a 3D-printed mechanical insect,” *Artificial Life*, vol. 17, no. 2, pp. 73–86, 2011.
- [4] R. C. Michelson and S. Reece, “UPDATE ON FLAPPING WING MICRO AIR VEHICLE RESEARCH Ongoing work to Develop a Flapping Wing, Crawling ”Entomopter”,” in *13th Bristol International RPV Conference*, Bristol, 1998.
- [5] J. A. Farnsworth, J. C. Vaccaro, and M. Amitay, “Aerodynamic performance modification of the Stingray UAV at low angles of attack,” in *Collection of Technical Papers - AIAA Applied Aerodynamics Conference*, vol. 3. American Institute of Aeronautics and Astronautics Inc., 2007, pp. 1686–1704.

- [6] G. A. Williamson, “EXPERIMENTAL WIND TUNNEL STUDY OF AIRFOILS WITH LARGE FLAP DEFLECTIONS AT LOW REYNOLDS NUMBERS,” Ph.D. dissertation, University of Illinois at Urbana-Champaign, Urbana-Champaign, 2012.
- [7] D. Artzi and E. Kroll, “LESSONS FROM WIND TUNNEL MODELS MADE BY RAPID PROTOTYPING,” *Rapid Prototyping Journal*, vol. 17, no. 5, 2011.
- [8] J. Scanlan and A. Keane, “SULSA - Southampton University Laser Sintered Aircraft,” 2011. [Online]. Available: https://www.southampton.ac.uk/~decode/index_files/Page804.htm
- [9] N. A. Ahmed and J. R. Page, “Manufacture of an unmanned aerial vehicle (UAV) for advanced project design using 3D printing technology,” *Applied Mechanics and Materials*, vol. 397-400, pp. 970–980, 2013. [Online]. Available: <https://www.scientific.net/AMM.397-400.970>
- [10] M. Ferraro, A. Lock, J. P. Scanlan, and A. J. Keane MFerraro, “Design and flight test of a civil unmanned aerial vehicle for maritime patrol: the use of 3D-printed structural components,” in *4th Aircraft Structural Design Conference*, Belfast, 2014. [Online]. Available: <https://eprints.soton.ac.uk/374202/>
- [11] M. J. Muir, E. J. Kolb, A. T. Parkinson, G. A. Robertson, C. L. Muldal, O. Querin, R. W. Hewson, and V. Toropov, “The Use of MDO and Advanced Manufacturing to Demonstrate Rapid, Agile Construction of a Mission Optimized UAV,” in *54th AIAA/ASME/ASCE/AHS/ASC Structures, Structural Dynamics, and Materials Conference*, Boston, 2013, pp. 1–21.
- [12] S. W. Miller, M. A. Yukish, M. E. Hoskins, L. A. Bennett, and E. J. Little, “A Retrospective Analysis of System Engineering Data Collection Metrics for a 3D Printed UAS Design,” in *Procedia Computer Science*, vol. 153. Elsevier B.V., 2019, pp. 1–8.
- [13] S. W. Miller, M. E. Hoskins, L. A. Bennett, E. J. Little, and M. A. Yukish, “CHALLENGES AND LESSONS LEARNED FROM DEVELOPING AN OPERATIONALLY RESPONSIVE 3D PRINTED UAV,” Penn State University, Tech. Rep., 2020. [Online]. Available: <https://scholarsphere.psu.edu/resources/80adcde0-b62f-4cfb-8cd4-0a69e196e504>
- [14] T. Jones, “ADDITIVELY MANUFACTURED COMPLIANT MECHANISM DESIGN AND APPLICATION FOR SUAS CONTROL SURFACES,” University Park, 2021.
- [15] S. Easter, J. Turman, D. Sheffler, M. Balazs, and J. Rotner, “Using advanced manufacturing to produce unmanned aerial vehicles: a feasibility study,” in *Ground/Air Multisensor Interoperability, Integration, and Networking for Persistent ISR IV*, vol. 8742. SPIE, 5 2013, p. 874204.
- [16] M. Stearn and E. Cohen, “VAST AUAV (variable airspeed telescoping additive unmanned air vehicle),” in *Rapid 2013 Conference and Exposition, Including 3D Imaging. SME.*, Pittsburgh, 2013.

- [17] “Stratasys Partners with Aurora Flight Sciences to Design and Develop the World’s First 3D Printed Jet-Powered Aircraft,” 11 2015. [Online]. Available: <https://www.stratasys.com/resources/search/case-studies/aurora>
- [18] “3D Lab Print.” [Online]. Available: <https://3dlabprint.com/>
- [19] “PLANEPRINT.” [Online]. Available: <https://www.planeprint.com/>
- [20] “3DAeroventures.” [Online]. Available: <https://www.3daeroventures.com/>
- [21] “Eclipsion 3D Printed Airplanes.” [Online]. Available: <https://www.eclipsion-airplanes.com/>
- [22] “Lofted Aero.” [Online]. Available: <https://www.loftedaero.com/>
- [23] “rc3Dprint.” [Online]. Available: <https://www.rc3dprint.com/>
- [24] “OWLplane.” [Online]. Available: <https://owlplane.com/>
- [25] “Kraga 3D printed RC planes.” [Online]. Available: <https://3dprintedrcplanes.com/>
- [26] “Nomad, an FPV/UAV 3D printed airplane,” 2014. [Online]. Available: <https://www.thingiverse.com/thing:272478>
- [27] Eclipsion, “Free RC airplane,” 2019. [Online]. Available: <https://www.thingiverse.com/thing:3302937>
- [28] J. D. Valenti and M. A. Yukish, “Design of Curvilinear Spars for Wings using 1D Loading Distributions,” in *AIAA Science and Technology Forum and Exposition, AIAA SciTech Forum 2022*. American Institute of Aeronautics and Astronautics Inc, AIAA, 2022.
- [29] J. D. Valenti, J. Bartolai, J. A. Cole, and M. A. Yukish, “Additive Manufacturing Process-Induced Wing Deformation and Effects on Aerodynamic Performance [ACCEPTED, PENDING PUBLICATION],” in *ASME International Mechanical Engineering Congress & Exposition*, Columbus, 2022.
- [30] “FARO Edge and FARO Laser ScanArm Edge Manual,” FARO, Tech. Rep., 2016. [Online]. Available: <https://downloads.faro.com/index.php/s/N95m3Hi8LZQw4FP?dir=undefined&openfile=39807>

Nomenclature

AM	Additive Manufacturing
c	Wing chord, m
CMM	Coordinate measuring machine
d_x	Spar spacing, chordwise distance between spars, mm
d_u	unsupported-wall distance, distance that a thin wall spans between supports, mm
G	List GCode points, $G = (g_1, g_2, \dots, g_n)$

MEAM	Material Extrusion Additive Manufacturing
P	List point cloud points, $P = (p_1, p_2, \dots, p_n)$
r	Ratio of unsupported-wall distance to extrusion width
RMS	Root Mean Square
UAV	Uncrewed Aerial Vehicle
w_e	Extrusion Width, mm
$w_{e,d}$	Designed Extrusion Width, mm
$w_{e,m}$	Measured Extrusion Width, mm
x	Chordwise coordinate, mm
y	Spanwise coordinate, mm
z	Vertical coordinate, mm
δ	Deformation, mm
η	unsupported-wall index, $(\kappa/d_u)w_e^2$
κ	Curvature, m^{-1}